# In-situ approach for thermal energy storage and thermoelectricity generation on the Moon: Modelling and simulation

Patrick Fleith [a,b,*], Aidan Cowley [a], Alberto Canals Pou [a,c], Aaron Valle Lozano [a,d,e], Rebecca Frank [a], Pablo López Córdoba [a,g], Ricard González-Cinca [f]

[a] European Astronaut Centre (ESA/EAC), Linder Hoehe, D-51147, Cologne, Germany
[b] ISAE-SUPAERO, 10 Avenue Edouard Belin, 31400, Toulouse, France
[c] Department of Materials Science and Metallurgy (CMEM), ETSEIB, Universitat Politècnica de Catalunya (UPC), Avda. Diagonal 647, 08028, Barcelona, Spain
[d] Luleå University of Technology, RYMDCAMPUS 1, 98192, Kiruna, Sweden
[e] Université Toulouse III - Paul Sabatier, Route de Narbonne, 31330, Toulouse, France
[f] Department of Physics, Universitat Politècnica de Catalunya-BarcelonaTech, c/ E. Terradas 5, 08860 Castelldefels (Barcelona), Spain
[g] UPC Escola d'Enginyeria de Telecomunicació i Aeroespacial, Carrer d'Esteve Terradas, 7, 08860 Casteldefels, Barcelona

*Keywords:*
Thermal energy storage
Thermoelectric
MATLAB
Moon
ISRU

A B S T R A C T

Human, tele-operated rovers, and surface infrastructures are now being actively considered for lunar polar exploration. Current approaches to energy provision consider, among others, hybrid direct energy/chemical technologies, such as solar photovoltaic arrays, batteries, and regenerative fuel cells. Due to the long period of darkness on the Moon and the challenges this poses to the aforementioned conventional energy generation and storage technologies, there is a need to assess the potential of In-Situ Resources Utilization (ISRU) methods to enable or supplement long duration missions. We present a computational model (MATLAB) of a Thermal Energy Storage (TES) system coupled to drive a heat engine (Thermoelectric Generator) to produce electricity. The TES medium designed is based off processed lunar regolith, an abundant material present on the surface of the Moon. The architecture has been optimized to provide a minimum electrical power of 36 W per unit after 66 h of polar night, but the modular nature of the model allows other ranges of parameter to be simulated. A trade-off between this ISRU-based concept and conventional approaches for energy production and storage was performed and ranked TES and thermoelectricity generation as the least appropriate option. This result is valuable in a period of enthusiasm towards ISRU. It shows that processes exploiting extraterrestrial materials instead of Earth supplies are not systematically attractive. Despite the non-favorable performances for the proposed concept, some perspectives for the TES system are given as well as potential model improvements such as the need to assess the use of a Stirling heat engine.

## 1. Introduction

There is a renewed interest in returning astronauts to the Moon and establishing a sustainable human exploration capability on its surface. Indeed, the "Moon Village" concept was initiated by Jan Woerner, Director General of the European Space Agency (ESA), and is part of the vision of Space 4.0, a set of concrete actions for returning to the Moon in an environment for international cooperation and commercialization of space (ESA, 2016).

One of the greatest challenges in the exploration of the Moon, which is addressed from an ISRU perspective in this paper, is the storage of energy for missions involving lunar nighttime. Pragmatically, the rim of the Shackleton crater at the South Pole of the Moon is not only a key target of interest for science and exploration but it also allows substantial sun visibility (Gläser et al., 2017), which reduces the potential complexity and mass of a stand-alone power system. Due to the prohibitive cost of transportation of materials from Earth, there is a need to assess In-Situ Resources Utilization (ISRU) approaches for energy production and storage. As ISRU has been identified as a key element to facilitate sustainable presence of humans in outer space (on the Moon or Mars), numerical modelling and simulation can enable us to assess its potential, and to compare it with other approaches. It is expected that through a smart use of ISRU, most of the systems could be built out of locally available resources, which would drastically decrease the amount of equipment launched from Earth. Nevertheless, the use of ISRU

* Corresponding author. European Astronaut Centre (ESA/EAC), Linder Hoehe, D-51147, Cologne, Germany.
*E-mail address:* pfleith.pro@gmail.com (P. Fleith).

https://doi.org/10.1016/j.pss.2019.104789

technologies has sometimes been questioned (Rapp, 2013). In this paper we propose and model a system for thermal energy storage in processed lunar regolith and electricity generation by means of thermoelectric converters. The advantages and disadvantages of the system with respect to other approaches have been analyzed in order to determine if the proposed concept has merit. The paper is organized as follows:

**Abbreviations**

| | |
|---|---|
| ESA | European Space Agency |
| EVA | Extra-Vehicular Activity |
| ISRU | In-Situ Resources Utilization |
| ISS | International Space Station |
| PDE | Partial Differential Equation |
| SEC | Solar Energy Collector |
| TC | Thermocouple |
| TE | Thermoelectric |
| TEG | Thermoelectric Generator |
| TES | Thermal Energy Storage |
| TM | Thermal Mass |

- Section 2 describes a realistic exploration scenario in the South Pole of the Moon, and its challenges in terms of energy production and storage. The variable sunlight conditions are addressed, and a plausible illumination profile is derived.
- An ISRU-based concept for Thermal Energy Storage on the Moon associated with Thermoelectric Generators (TES/TEG) is introduced in Section 3.
- Section 4 describes an integrated MATLAB model of the TES/TEG concept. The description includes the assumptions, data, and equations that have been used to build the model, such as temperature-dependent properties of regolith and thermoelectric materials.
- A trade-off analysis is presented in Section 5, in which the TES/TEG concept is compared to power subsystems based off solar arrays and batteries, solar arrays and regenerative fuel cells, and fission surface power. The trade-off analysis has ranked the TES/TEG concept as the least favorable alternative. It suggests that the concept and technologies need significant improvements to become more practically attractive. Therefore, a list of recommendations to improve the model and some general perspectives regarding ISRU-based thermal energy storage are provided in Section 6.

## 2. Exploration scenario of the Moon and the challenge of energy production and storage

### 2.1. Reasons for exploration of lunar South Pole

One of the major challenges for a long duration human surface mission will be provision of energy due to protracted darkness during the nighttime. The synodic period of the Moon is 29.54 days (709 h) (Shrunk et al., 2008). At equatorial rons of the Moon, the lunar night can last up to 350 h which is much longer than in the ISS (eclipses of 45 min). Therefore, the energy to be stored in order to meet a similar power demand would significantly increase on the Moon. In case batteries were used for energy storage, its number would be at least two orders of magnitude larger than in the ISS, which would lead to a dramatic increase of mass to be launched from Earth. Lunar poles are rons that benefit from long periods of sunlight due to the low elevation angle of the Sun and local topography (Gläser et al., 2017). Therefore, photovoltaic panels could be used for long periods, which would reduce the energy to be stored for the dark periods.

The polar temperature variations can be smaller at lunar poles (50 °C) than at the equator (250 °C) (Paige et al., 2010) which is an advantage for materials and infrastructures which are sensitive to degradation from high-amplitude thermal cycling (Shrunk et al., 2008). However, the local topography and sun elevation at the poles could cause the number of thermal cycles to be greater than elsewhere on the Moon which affects planetary systems design.

Several lunar observation missions delivered evidence of the presence of water in the form of ice located in permanently shadowed rons near poles. Volatile water can be trapped in cold places such as these rons. The LCROSS mission estimated a mass concentration of water ice in the regolith of $5.6 \pm 2.9\%$ (Colaprete et al., 2010). Water is of high importance to support human presence since drinkable water can be obtained from it, and $O_2$ and $H_2$ can be obtained by means of electrolysis.

The primary interest for lunar surface missions is the access to relevant terrains for science and exploration preparation, whereby geological, geophysical and geochemistry research can be performed and exploration enabling technologies can be demonstrated in-situ. In addition, the aforementioned reasons for exploration of lunar South Pole are strong enablers for mission feasibility.

### 2.2. Determination of the illumination profile at the rim of the Shackleton crater

In order to study the potential of a solar-based concept for energy production and storage, it is necessary to identify the illumination profile at the target location. The South Pole presents some sites with high levels of sun visibility. These areas are located near the Shackleton crater, as depicted by the illumination map in Fig. 1. They present high solar visibility, and a maximum continuous polar night significantly shorter than at equatorial rons.

In the considered scenario, any asset placed on the Moon's surface would experience a period of darkness between 100 and 250 h maximum. However, 2 m above the surface, the illumination conditions are much better. At a position of latitude −89.6866°N and longitude 197.19°E, the solar visibility is estimated to be 89.4% (over a 20-year period) and the maximum time continuously in shadow is 66 h (Gläser et al., 2017). This illumination condition represents therefore the best-case scenario (in term of longest darkness period) to study the feasibility of the concept. We assume that the solar energy collector would be mounted 2 m above the surface in order to increase solar visibility. This is possible since quantitative values are available from the literature as an input to our analysis (Gläser et al., 2017). One might argue that, instead, the worst illumination case scenario should be assessed. However, since the objective of this work is to determine if the proposed concept has merit, any negative assessment in the best-case scenario would also eliminate the choice of this power supply alternative for harsher conditions.

## 3. Thermal energy storage concept for electricity generation

An ISRU approach as a means of energy provision is to use the lunar regolith as the medium for thermal energy storage (Balasubramaniam et al., 2010a; Climent et al., 2014), similar to the underground thermal energy storage concept used on Earth. Heat can be stored in solid materials (thermal mass) in the form of sensible heat. A hot heat transfer fluid passes through the thermal mass heating it. If the heat losses are minimized, the thermal mass can be kept at high temperature, until the energy is released using the reverse mechanism. In this case, a cold working fluid passes through the thermal mass and absorbs the heat. The temperature of the fluid increases, which can be used as the source for a heating system.

The thermal masses can be fabricated at the Moon using sintered regolith. Sintering is accomplished by compacting loose material (powders, lunar dust) and forming a solid mass of material by applying heat and/or pressure. During this process, particles form strong bonds with a reduction in the volume of pores, with an attendant change in other

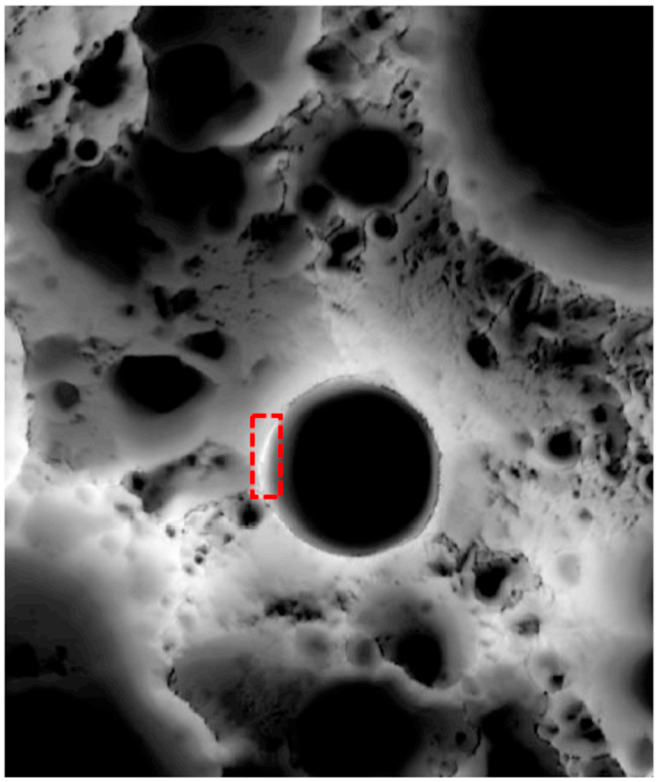

**Fig. 1.** Multi-temporal illumination map of the lunar South Pole. The Shackleton crater (19 km diameter) is in the center. The South Pole is located approximately at 9 o'clock on its rim (highlighted ron). Mapped area extends from 88°S to 90°S (NASA/GSFC, 2010).

material characteristics (e.g. bulk thermal conductivity). It has been demonstrated on Earth that lunar regolith simulant can be processed into solid blocks (lunar bricks) with higher thermal conductivity than native regolith (by a factor 200). A 1.5 tons block made of lunar regolith simulant was 3D printed for proof of principle demonstration at the European Space Agency (ESA, 2010).

Fig. 2 shows the proposed energy storage concept coupled with a heat engine. The concept is based on the thermal energy storage systems proposed in (Balasubramaniam et al., 2010a; Climent et al., 2014). The system contains the following components: a solar energy concentrator to focus the incident sunlight and achieve a high heat flux; a thermal mass made of sintered regolith which is heated by the concentrated flux; a heat engine that converts the thermal energy into electricity, and a radiator that keeps the cold sink at low temperature. The different subsystems are described in the following modelling section.

## 4. Modelling the TES/TEG system

This section details the assumptions, data, and equations used to build the model for further assessment of the potential of the TES/TEG concept. The model has been implemented in MATLAB R2017b (Fleith, 2017).

### 4.1. Modelling the solar energy collector

The objective of the Solar Energy Collector (SEC) is to collect and concentrate the solar flux to reach the high temperature desired for the thermal mass to store energy. The SEC is composed of a reflector and a concentrator. The reflector consists of a reflective mirror surface that can track the Sun position. The reflector is able to re-direct a high incidence flux perpendicularly to the target surface. Since a normal incidence flux is not sufficient, a Fresnel lens can be used to concentrate the Sun flux (Turner, 1983).

We assume that a reflector can ensure a minimum flux of 1000 $W.m^{-2}$ during the polar day. This is acceptable given the general incoming solar flux on the Moon (neglecting ephemeris variations) is $\phi_{sun} = 1365\ W.m^{-2}$. The assumed lower value of the flux provided by the reflector accounts for efficiency of the mirrors (secular reflectivity estimated to be 85–90%), misalignments, actuation and geometrical limits. Thus, the heat flux given by the reflector is:

$$\phi_R = \begin{cases} 1000\ W.m^{-2} & (in\ sunlight) \\ 0\ W.m^{-2} & (in\ shadow) \end{cases} \quad (1)$$

The concentrated flux of the SEC is given by:

$$\phi_C = f \cdot \eta_{FL} \cdot \phi_R \quad (2)$$

where $f$ is the magnification of the Fresnel lens and $\eta_{FL}$ its efficiency. With $f = 70$, a reflected flux of 1 $kW.m^{-2}$ can be concentrated to achieve almost 70 $kW.m^{-2}$. It is assumed that a magnification of $f = 70$ and only 5% of transmission losses can be achieved for a Fresnel lens optimized for the Moon. These assumptions are the basis for the concentrated solar flux and enable the top surface temperature of the thermal mass to reach about 1000 K (Lozano, 2016).

### 4.2. Modelling the thermal mass

The Thermal Mass (TM) thermally stores the energy and serves as a hot source for the heat engine. It is made of sintered regolith and buried into the lunar native regolith to mitigate heat losses. Indeed, the native regolith acts as insulator material, owing to its low thermal conductivity. No loop heat pipes were considered inside the TM since its conductivity is already enhanced with the sintering process. (average values of 2.1 $W.K^{-1}.m^{-1}$) for sintered regolith against 0.01 $W.K^{-1}.m^{-1}$) for native regolith (Colozza, 1991; Jones et al., 2011))

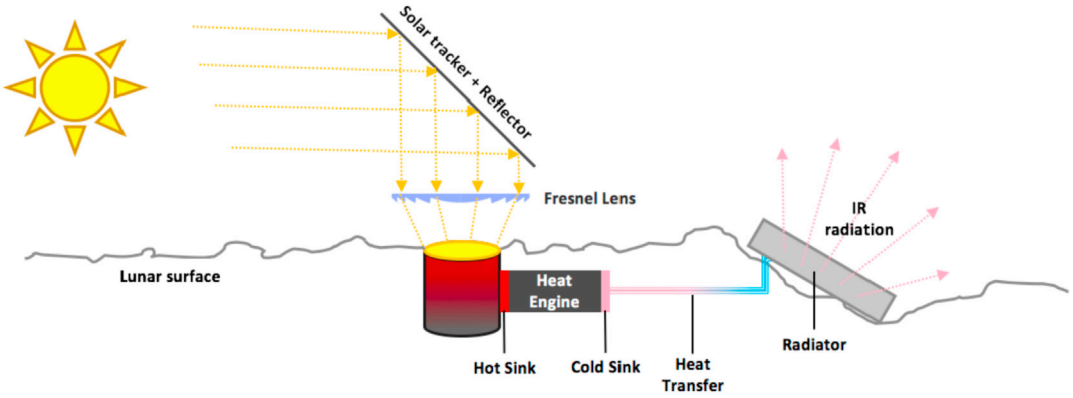


**Fig. 2.** Thermal Energy Storage system coupled with a heat engine for electricity generation, and a radiator to cool down the cold sink.

The model of the TM was implemented with the Partial Differential Equations (PDE) toolbox of MATLAB. A 2D-model is chosen because a vertical cross-section of the entire TM is sufficient to study the system. In previous studies, a cylindrical geometry of 0.5 m in height and 0.3 m in diameter was considered (Lozano, 2016; Córdoba, 2017). These values are closely linked to manufacturing capability of sintering methods. Because in this concept the TM is buried into lunar soil, automotive rovers or astronauts would have to drill and excavate native regolith. The level of difficulty to perform this operation for depths greater than 0.5 m – 1m is not well known. Sintering lunar rovers would also have limited size. Therefore, the diameter is set to 0.3 m. These values were initially used for the model and ultimately set to a depth of 0.65 m and width of 0.3 m for optimized performances.

Fig. 3 shows the designed TM buried into native regolith. At the top of the native regolith, a 'fluff' layer of regolith is modelled (with a very low thermal conductivity, see Table 1 and Equation (7)). On each side of the TM, an interface (hot sink plate) is modelled, and a hole is defined within this geometry to model the presence of a TEG module. The overall model does not have a meshed TEG since all computations for thermal transfers are done with a TEG MATLAB function. We assume that the cold side of the TEG is connected to a cold plate which rejects the heat through the radiator. Heat transfer from the TEG cold side to the radiator are not implemented in this geometry since it is implemented in a separate function. Additionally, a thermal conductance beam is modelled vertically in the middle of the TM in order to enhance heat propagation through the medium. Although sintered regolith has a larger thermal conductivity than fluff regolith, and thus a larger heat transfer rate, the optimization process of this work showed that the presence of a thermal beam substantially increases the system performance.

The PDE toolbox automatically generates the mesh and increases the number of nodes where it is needed (see Fig. 3).

The thermal mass model element can return the temperature at any time during the simulation as we solve a transient heat transfer problem with temperature dependent properties. The model accounts for heat gain from the Sun, losses, and energy extracted for power generation. The associated partial differential equation to be solved for conductive heat transfer is:

$$\rho \cdot c_p(T) \cdot \frac{\partial T}{\partial t} - \nabla \cdot (\kappa(T) \cdot \nabla T) = h, \tag{3}$$

where $\rho$ is the density of the body, $c_p(T)$ its specific heat, $T$ is the body's temperature, $\kappa(T)$ its thermal conductivity, and $h$ is the heat generated inside the body. In order to solve Eq. (3), the properties of sintered regolith, native regolith, and fluff layer are provided as inputs (Table 1). The surface emissivity of sintered regolith is assumed to be similar to native regolith emissivity. The surface absorptivity is assumed to be 0.85 since the Moon albedo ranges from 0.1 to 0.2 and the mean value for the surface of the Moon is 0.15 (Vasavada et al., 2012). During the polar night, the surface emissivity of the TM is reduced by a factor 50 in order to account for radiative losses mitigation. This can be practically done by employing a highly reflective/insulating cover cap which covers the top of the TM during the polar night. This could be made with Multi-Layer Insulation (MLI) which has a high insulating performance ($0.0006\ \mathrm{W.K^{-1}.m^{-1}}$ for a 40-layer MLI) (Rapp, 2013).

It is important to implement the temperature dependence of the TM properties due to the large temperature variations. An expression for TM conductivity was obtained from a curve fit and interpolation of experimental data provided in the literature for the specific case of sintered lunar rock (resolidified) (Colozza, 1991; Hemingway et al., 2481):

$$\kappa_{TM}(T) = 6 \times 10^{-7} \cdot T^2 - 0.0028 \cdot T + 3.3753 \tag{4}$$

Similarly the specific heat for lunar sintered regolith has been fitted to the following expression (Colozza, 1991; Langseth et al., 1976):

$$c_{pTM}(T) = -5 \times 10^{-4} \cdot T^2 + 1.4332 \cdot T + 371.5 \tag{5}$$

The native regolith conductivity (Vasavada et al., 1999; Mitchell and De Pater, 1994):

$$\kappa_{nat}(T) = 0.0093 \cdot \left\{1 + 0.073 \cdot \left(\frac{T}{350}\right)^3\right\} \tag{6}$$

The fluff regolith layer conductivity (Vasavada et al., 1999; Cremers, 1973):

$$\kappa_{fluff}(T) = 9.22 \times 10^{-4} \cdot \left\{1 + 1.48 \cdot \left(\frac{T}{350}\right)^3\right\} \tag{7}$$

Eqs. (3)–(7) and Table 1 are used to compute the conductive heat transfer between the thermal mass and the surrounding regolith. Convection mechanism are not considered since there is nearly vacuum on the Moon. The remaining losses are radiative heat losses, which are given by:

$$\phi_{rad} = \varepsilon_{TM} \cdot \sigma \cdot \left(T_{top}^4 - T_{space}^4\right), \tag{8}$$

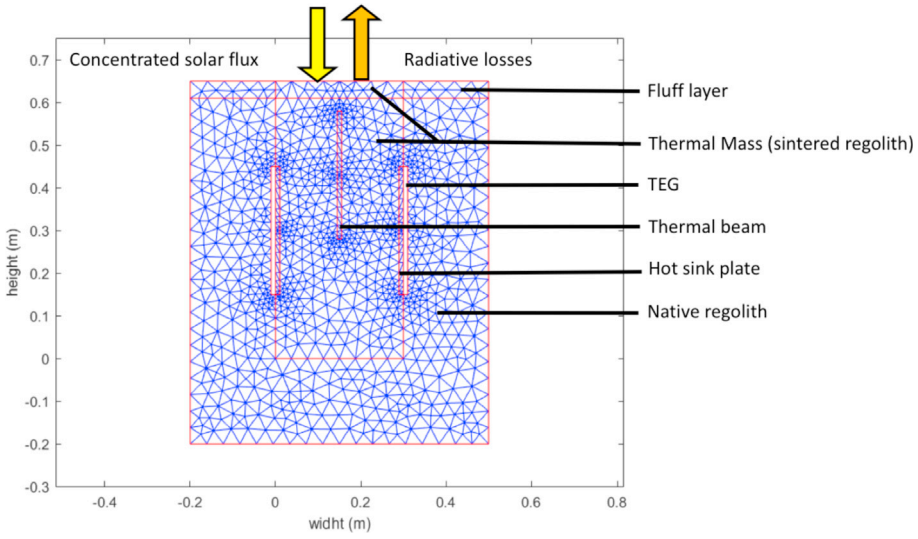


**Fig. 3.** 2D-Model of the TM buried into lunar native regolith with a thermal beam in the middle and TEG modules on each side (white rectangles) attached to the hot sink plates. Note that the fluff layer does not extend on the top of the TM. The rectangle at the top of the TM is actually part of the sintered regolith block as pointed out on the figure.

**Table 1**
Properties of native and fluff regolith. Sintered regolith properties are taken similar to basalt rock.

| Properties | Native Regolith | Fluff layer | Sintered Regolith (basalt rock) |
|---|---|---|---|
| Density ($kg.m^{-3}$) | 1800 (Balasubramaniam et al., 2010a) | 1300 (Mellon et al., 2000; Heiken et al., 1991) | 3000 (Balasubramaniam et al., 2010a) |
| Specific heat ($J.kg^{1}.K^{-1}$) | 840-850 (Balasubramaniam et al., 2010a; Colozza, 1991) | 840-850 (Balasubramaniam et al., 2010a; Colozza, 1991) | 800 (Balasubramaniam et al., 2010a) |
| Thermal conductivity ($W.K^{-1}.m^{-1}$) | $9.3 \times 10^{-3}$ (Balasubramaniam et al., 2010a; Colozza, 1991) | $2.29 \times 10^{-3}$ Mellon et al. (2000) | 2.1 (Balasubramaniam et al., 2010a) |
| Surface emissivity ( – ) | 0.96 (Vasavada et al., 1999) | 0.96 (Vasavada et al., 1999) | 0.96 (Vasavada et al., 1999) |
| Surface absorptivity ( – ) | 0.85 (Vasavada et al., 2012) | 0.85 (Vasavada et al., 2012) | 0.85 (Vasavada et al., 2012) |

where $\phi_{rad}$ is the radiative flux, $\varepsilon_{TM}$ is the emissivity of the TM, $\sigma$ is the Stefan-Boltzmann constant ($5.67 \times 10^{-8}$ $W.m^{-2}K^{-4}$), $T_{top}$ is the temperature of the top surface of the TM facing outer space, $T_{space}$ the temperature of deep space usually taken at 3 K. During the polar night $\varepsilon_{TM}(night)$ is taken as $\varepsilon_{TM}(day)/50$.

In order to compute the temperature in the TM, an initial temperature of the system has to be selected. 254 K is the bulk temperature beyond the thermal penetration depth of the lunar soil. The penetration depth usually ranges from 0.2 to 0.3 m. Therefore, the bottom boundary of the TM is set at a constant temperature of 254 K. To fix a constant temperature on a boundary, a *Dirichlet* boundary condition is employed in MATLAB.

The TM model also takes into account heat gain from the Sun flux and heat losses towards deep space (conduction losses are directly simulated by the model since native regolith surrounds the TM geometry). The TM receives a constant flux from the SEC during the polar day given by:

$$\phi_{SEC \to TM} = \alpha_{TM} \cdot \phi_C \tag{9}$$

$\alpha_{TM} = 0.85$ being the absorptivity of the TM.

The net flux absorbed by the element is given by $\phi_{SEC \to TM}$ and the radiation losses:

$$\phi_{net}(T) = \phi_{SEC \to TM} - \phi_{rad}(T) \tag{10}$$

$\phi_{net}(T)$ is set as a *Neumann* boundary condition in MATLAB at the top surface of the TM.

The general form of the partial differential equation solved by the MATLAB PDE Toolbox is:

$$m \frac{\partial^2 u}{\partial^2 t} + d\frac{\partial u}{\partial t} - \nabla \cdot (c\nabla u) + au = z, \tag{11}$$

where in our model u corresponds to temperature and the coefficients are given by: $m = 0$, $d = \rho \cdot cp(T)$, $c = \kappa(T)$, and $z = h = 0$ (no heat generated in the system).

Unlike PDE's coefficients, *Neumann* boundary conditions cannot be set as temperature-dependent in the PDE toolbox of MATLAB. In order to overcome this problem, the simulation computes the temperature profile with a value of $\phi_{net}$ that is updated with the new temperature values at the end of each time step in the code. The time step was kept below 100 s due to convergence issues if exceeding 120 s.

### 4.3. Modelling the thermoelectric generator

The Thermoelectric Generator (TEG) consists of an array of thermocouple materials assembled in series, sandwiched into two plates: one hot and one cold sink plates. The plates serve as interfaces between the thermoelectric array: on one side with the hot thermal mass, and on the cold side with the radiator where the wasted energy is dissipated (see Figs. 2 and 3). These plates are assumed to be a thin interface made of conductive material in order to provide a homogeneous temperature for all thermocouples attached to it. Aluminum prevails in lunar regolith, mostly in form of oxides. Therefore, due to its high thermal conductivity and availability on-site, Aluminum was chosen as a good test candidate for the plates (see properties of Aluminum in Table 2). A conservative value for the thermal conductivity is taken to account for impurities and performance degradation due to thermal cycling.

The performance of a thermocouple depends on the working temperature, and the temperature difference between the hot and cold plates. For this section, modelling strates employed previously (Alam and Ramakrishna, 2012; Tsai and Lin, 2009; Termo-Gen, 2006; Kanimba and Tian, 2016; Tatarinov et al., 2013; TEC Solidstate Power Generators, 2016; Romanjek et al., 2015) have been used.

The temperature difference between the hot and the cold plate ($\Delta T = T_h - T_c$) leads to the open circuit voltage $V_{oc} = S(T_m) \cdot \Delta T$ due to the Seebeck effect given by

$$S(T_m) = |S_n(T_m)| + |S_p(T_m)|, \tag{12}$$

where $S(T_m)$ is the Seebeck coefficient, which depends on the mean temperature between the hot and cold side, $T_m$ . $S_n(T_m)$ and $S_p(T_m)$ are the Seebeck coefficients for the n-type and p-type semiconductors, respectively. The value of $S(T_m)$ can be found in the literature and enables computation of the open circuit voltage:

Considering $n$ thermocouples assembled in series, the open circuit voltage for the TEG is given by $U_{oc} = n \cdot V_{oc}$.

Each thermocouple is made of one n-type and p-type leg with resistivity $\rho_n$ and $\rho_p$ , respectively, which depend on the mean temperature. Therefore, the internal resistance of one thermocouple is:

$$R_i = \left[\rho_n(T_m) + \rho_p(T_m)\right] \cdot \frac{h_{leg}}{A_{leg}}, \tag{13}$$

$h_{leg}$ being the height of the leg (4.9 mm) and $A_{leg}$ its area (2.5 mm * 2.5 mm) only for the case of SiGe based thermocouples. Other thermocouples use a fixed resistance given in their datasheets. The internal resistance for the TEG made of $n$ thermocouples assembled in series is:

$$R_{i\ TEG} = n \cdot R_i \tag{14}$$

To maximize the power output from the TEG, the load resistance $R_{L\ TEG}$ (the resistance of the electrical system attached to the TEG) has to match the internal resistance, $R_{L\ TEG} = R_{i\ TEG}$. Thus, the load current $I_L$ and voltage $U_L$ are:

$$I_L = \frac{U_{oc}}{R_{i\ TEG} + R_{L\ TEG}} \tag{15}$$

$$U_L = U_{oc} - I_L \cdot R_{i\ TEG} \tag{16}$$

The output power provided by the TEG module is given by $P_{elec}$ =

**Table 2**
Properties of Aluminum used to model the hot and cold sink plates (Morrel, 2018; Callister and Rethwisch, 2007).

| Properties | Hot/cold Sink Plate |
|---|---|
| Density (Al) ($kg.m^{-3}$) | 2700 |
| Specific heat (Al) ($J.kg^{-1}.K^{-1}$) | 900 |
| Thermal conductivity (Al) ($W.K^{-1}.m^{-1}$) | 150 |
| Thickness of plate (m) | 0.01 |
| Aluminum melting point (K) | 932 |

$U_L \cdot I_L$.

Although the TEG module produces electricity out of the TM (hot source), one must consider that it also absorbs heat from it. This absorbed heat reduces the temperature of the TM during the polar night, which in turn decreases the temperature gradient across the TEG needed for electricity production. This negative retroactive effect has been considered in our study.

To obtain the relationships for the absorbed and rejected power in the TEG, three heat transfer mechanisms inside the thermocouple shall be considered. The Fourier process based on the material conductivity $\kappa$ and the temperature difference $\Delta T$ between each side; the Joule heat dissipated due to current flows $I_L$ and internal electrical resistance $R_i$ ; and the Peltier cooling/heat effect which is the phenomenon of heat absorption or dissipation at the junction of two dissimilar materials when an electrical current flow through this junction (Tsai and Lin, 2009). The heat absorbed or rejected based on the Peltier effect is given by $S(T) \cdot I_L \cdot T_{h \text{ or } c}$. The combination of these three mechanisms for $n$ thermocouples, gives the power absorbed at the hot side, and the power rejected at the cold side:

$$P_{abs} = n \cdot \left\{ -\frac{1}{2} \cdot R_i \cdot I_L^2 + S(T_m) \cdot I_L \cdot T_h + \kappa \cdot \Delta T \right\} \tag{17}$$

$$P_{rej} = n \cdot \left\{ \frac{1}{2} \cdot R_i \cdot I_L^2 + S(T_m) \cdot I_L \cdot T_c + \kappa \cdot \Delta T \right\} \tag{18}$$

The material thermal conductivity is often missing in TEG datasheet. However, it can be extracted from $\kappa = \frac{S(T_m)^2}{R_i \cdot Z}$, where $Z = \frac{Z_T(T_{hot})}{T_{hot}}$, $Z_T$ being the figure of merit. Therefore, the following parameters are required to compute all outputs: $T_{hot}$, $T_{cold}$, $n$, $Z_T(T_{hot})$, $R_i$ or $R_i(T_m)$ and S or $S(T_m)$.

In the present case, three thermoelectric materials ($Bi_2Te_3$ (Term-o-Gen, 2006), PbTe/TAGS (TEC Solidstate Power Generators, 2016), and SiGe (Romanjek et al., 2015)) have been considered and their properties are summarized in Table A.1 of Appendix A. The model of the TEG was implemented as a MATLAB function.

The TEG function was validated with the performance reported in the literature. The error in the simulated power output with respect to the datasheet is less than 2.5% for $Bi_2Te_3$ and PbTe/TAGS. For SiGe-based TEG, the simulated power output is within the uncertainty range presented in (Romanjek et al., 2015).

### 4.4. Modelling the cooling subsystem

The Cooling Subsystem (CS) works as follows: a cold plate absorbs the heat rejected by the thermoelectric generator, and the heat is evacuated to the radiator. As for the hot side, the chosen material is Aluminum. The temperature of the cold plate is computed as the temperature of the radiator assuming an ideal transfer of the TEG rejected heat. The chosen initial temperature in order to simulate the polar day is 250 K.

The radiator receives heat from the TEG and dissipates it towards the cold deep space. Thus, it is thermally coupled with space and the Moon's surface. Each contribution depends on the radiator geometry and orientation (view factors), the topography of the site, and the temperature profile of the lunar soil at that place. An ideal location for the radiator at the South Pole would be a permanent or long shadowed ron. In this case, the radiator will achieve maximum performance due to the low environment temperature.

The radiator is assumed to be made of Aluminum. A coating surface is considered to maximize emitted heat flux, $\varepsilon_{rad}$ , and minimize absorbed solar flux, $\alpha_{rad}$. At bnning-of-life, common values for white epoxy materials are $\varepsilon_{rad} = 0.9$ and $\alpha_{rad} = 0.25$ (Nicollier, 2019). However, due to solar high-energy radiation (UV), most of the coatings age over time and, degraded sizing values were used: $\varepsilon_{rad} = 0.8$ and $\alpha_{rad} = 0.4$. These values do not account for lunar dust depositing onto the radiator which could affect its overall emissivity and absorptivity.

The evolution of the temperature of the radiator is given by:

$$\frac{dT_{rad}}{dt} = \frac{1}{m_{rad}\ c_{p\,rad}} \cdot \left(P_{rej} + P_{sun} - P_{radiator \to space} - P_{radiator \to moon}\right), \tag{19}$$

where $m_{rad}$ is the mass of the radiator, $c_{p\,rad}$ is the specific heat of Aluminum, $P_{sun}$ is the incoming power from the solar irradiance, $P_{radiator \to space}$ is the radiative power losses towards space, and $P_{radiator \to moon}$ is the net power transferred to the Moon surface. This latter contribution is assumed to be negligible, due to temperature equilibrium between the radiator placed directly on the fluff insulating regolith, and the possibility of carefully selection of the coating material. $P_{sun}$ is given by:

$$P_{sun} = A_{rad} \alpha_{rad} \phi_{sun}, \tag{20}$$

$A_{rad}$ being the area of the radiator, $\alpha_{rad}$ the absorptivity of the coating, and $\phi_{sun}$ the direct sun irradiance. On the poles the maximum sun elevation is about 1.54° which would lead to an irradiance of 37 $W.m^{-2}$. However, direct solar irradiance has been taken 100 $W.m^{-2}$ as a worst-case value. This is to account for non-flatness of the local terrain which could cause the maximum sun elevation with respect to the radiator plane to be higher than expected at the poles. The radiator size needed is about 10 $m^2$.

The radiative power loss to space is given by:

$$P_{radiator \to space} = f_{rs} A_{rad} \varepsilon_{rad} \sigma \left( {T_{rad}}^4 - {T_{space}}^4 \right), \tag{21}$$

where $f_{rs}$ is the view factor considered equal to one (radiator placed horizontally on the lunar surface).

The change in temperature of the radiator (and thus the cold side) in a simulation time step $\Delta t$ is finally given by:

$$\Delta T_{cold} = \Delta T_{rad} = \frac{1}{m_{rad}\ c_{p\,rad}} \cdot \left(P_{rej} + P_{sun} - P_{radiator \to space}\right) \cdot \Delta t \tag{22}$$

## 5. Results and discussion

### 5.1. Performances optimizations and results

For the proposed TES/TEG concept, the main performance drivers have been identified through a fractional factorial design. Preliminary simulations have shown that the temperature experienced by the TEG at the hot sink is close to 410 K at the end of the polar night. Given this specific temperature differential (240 K) between the hot and cold plates and the cold plate temperature at the end of the darkness period (170 K), $Bi_2Te_3$ shows an efficiency (9.3%) higher than PbTe/TAGS (<9%) or SiGe (<3%). $Bi_2Te_3$ is the most obvious suitable material unless further materials are implemented in the model. It is worth mentioning that in the case of $Bi_2Te_3$, temperature-dependent properties were not available from the datasheet. However, due to the modularity of our model, it can be added in the future for better accuracy of results.

The influence of seven factors on the performance of the system was analyzed. The following four factors showed a significant influence:

- The power output of a TES/TEG unit at the end of a polar night is improved when the height of the TM it is set at 0.65 m rather than at 1 m.
- The ability of the cover cap to mitigate radiative losses. The model gave much better performance with a TM emissivity reduced by a factor 50 than with a TM emissivity reduced only by a factor 10 during the polar night.
- The achievable cold temperature plays an important role: 170 K at the cold side instead of 200 K significantly increases the power output.
- The presence of a thermal beam inside the TM substantially improved the system performance. Optimization of the dimension and location of this beam for better performances is left for future works. It is currently a preliminary design which gives a good compromise between performances improvement and mass of the thermal beam.

Other studied factors which had a negligible influence are:

- The surface occupied by the TEG (0.2 or 0.3 $m^2$), which impacts the absorbed heat flux.
- The depth at which the TEG is placed in the TM (0.2 or 0.3 m from the TM surface).
- The number of thermocouples per TEG (50 or 80).

Thanks to the identification of the main performance drivers, an ultimate simulation is performed which leads to the best performance of the system in the considered scenario. The numerical simulations reproduced the behavior of the system during 150 h of concentrated sunlight followed by 66 h of darkness. The results are presented in Fig. 4 and Fig. 5.

A steady temperature is reached at the end of the polar day (Figs. 4a and 5a). The top of the thermal mass reaches 1000 K while the bottom temperature stays at 600 K. This persistent gradient is explained by the relatively low thermal conductivity of sintered regolith, the heat absorbed by the TEG and the losses by conduction in native regolith.

At the end of the 66 h of polar night, the temperature in the TM is more homogeneous and decreases to about 420 K (Figs. 4b and 5a). The coldest spots are the rons near the TEGs (Fig. 4b), since each TEG plate absorbs between 200 W and 400 W from the TM (Fig. 5d).

The temperature difference achieved between the hot and the cold plates ranges from 240 K to 400 K (Fig. 5b). The peak observed after sunset is due to the sudden decrease of the cold plate temperature. This peak in turn results in a peak in the power output (Fig. 5c), the heat flow through each TEG element (Fig. 5d), and the efficiency of the TEG elements (Fig. 5e). The efficiency of the TEG is within the range of expected values for thermoelectric materials (8%–11%).

Similar to the TM temperature, the power output reaches a constant value during the polar day at approximately 42 W per TEG (Fig. 5c) and sharply decreases during the polar night. At the end of the darkness period, only 18 W are produced per TEG. Hence, the proposed concept which includes two TEG plates provides a minimum of 36 W at any time during the 66 h of darkness considered.

Fig. 5f shows the number of required elements to provide 10 kW to a surface payload with a very conservative 50% margin (accounting for a safety factor and low TRL technology). At the end of the polar night, approximately 420 elements are needed to provide the required power.

### 5.2. *Trade-off analysis*

Trade-off analyses are frequently used to evaluate the potential of various alternatives, in order to support a decision-making process. In the present case, the philosophy is to use it as a tool to assess objectively the potential of our scenario concept with respect to more conventional approaches. The analyzed systems are:

1) The TES/TEG system modelled in the present study.
2) A combination of solar panels and rechargeable batteries. This is the current approach used on-board the ISS and by most of space missions in the vicinity of the Earth.
3) A combination of solar panels and regenerative fuel cells. This is a promising system since fuel cells benefit from significant space heritage.
4) Fission Surface Power. An important advantage of this system is the continuous power production irrespective of the irradiance conditions, with a relatively compact system.

The trade-off analysis was performed considering the following criteria:

- **Mass of the power system:** Launch costs represent a significant part of any mission, and therefore a low-mass system is desirable given a fixed power requirement.

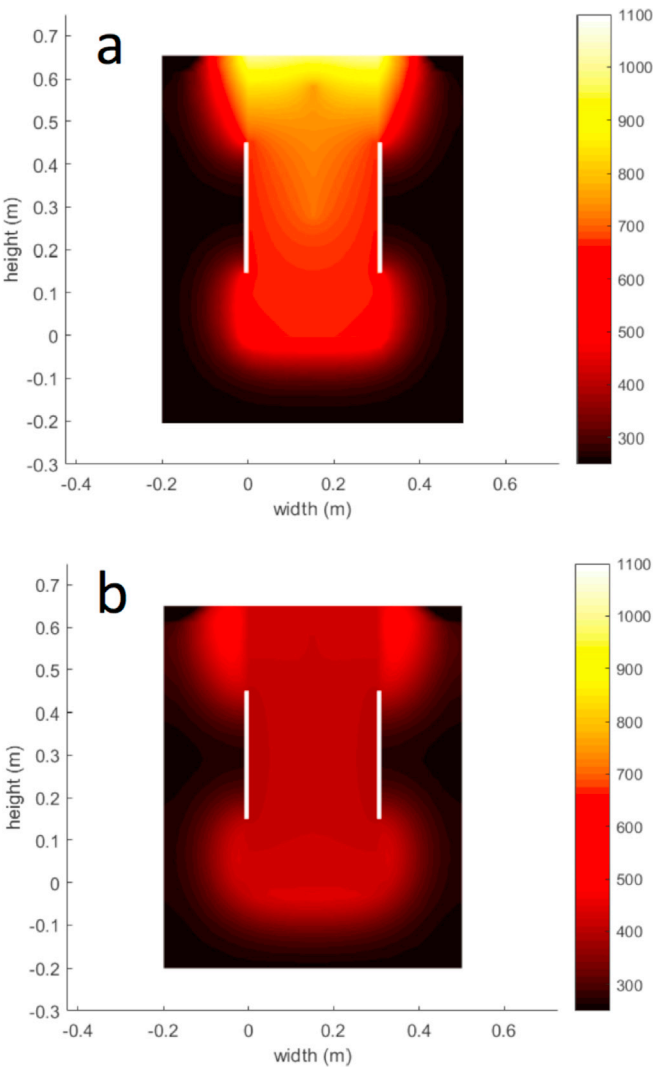


**Fig. 4.** Temperature profile (K) of the thermal mass (a) after 150 h of applied concentrated sunlight (b) after 66 h of radiative losses in the polar night. White rectangles are the TEG modules.

- **Global specific power**: Power output per unit of mass for the system. It is denoted as "global" since it is computed considering the global energy system mass (i.e. production units, storage mean, resources extracted from the Moon, structural elements, etc.). This criterion enables to assess the "compactness" of the system on the Moon.
- **Space heritage**: A space-proven technology is more likely to be used than a technology which requires years and considerable investment in research and technology development. The space heritage can be assessed using the technology readiness level scale (TRL).
- **System complexity:** All characteristics being equal, a simple system is a better solution than a complex system. Indeed, knowledge acquisition is easier, and more confidence is placed during operations and maintenance. Furthermore, the end users would be able to interact easily, modify and adapt the system depending on real on-site situations.
- **Installation efforts:** This criterion aims to quantify the level of efforts that needs to be placed into the installation in the energy system before being operational. Some systems may be ready to use, mechanically deployable, or "plug & play". Some others might require robotic assisted installation, extensive ISRU, or extra-vehicular activities (EVAs) on the Moon surface.
- **Operations:** This criterion encompasses daily work required for astronauts, robots, ground control center, but also maintenance of the

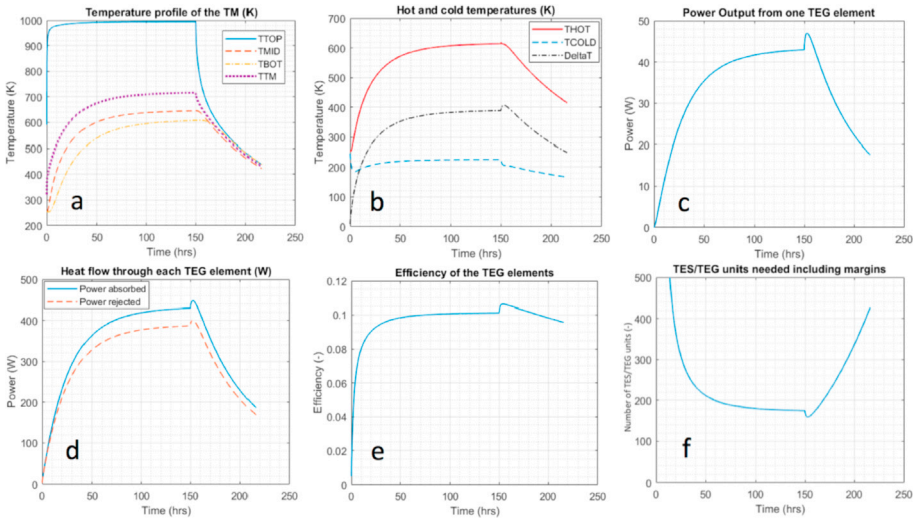


**Fig. 5.** (a) temperature profile of the TM at the top (TTOP), mid-height (TMID), bottom (TBOT), and mean value (TTM). (b) Temperature difference between the hot and cold plates (c) Power output of one TEG (d) Power absorbed and rejected at the hot and cold plate, respectively. (e) Efficiency of the TEG elements. f) Number of TES/TEG elements needed including 50% to comply with 10 kW power requirement of a Moon base.

system. Safety issues due to hazardous components will also complicate operations, maintenance or work nearby the system.

- **Scalability:** The power system not only aims to provide electrical power to the primary habitat, but might be used for surface robots, pressurized rovers, EVA systems. Moreover, new infrastructures will be progressively implemented and added to the main base in the "Moon Village". Thus, it is important for a power system to be versatile, to interface with all of these elements, and to be scalable for increasing or decreasing power demand.
- **Lifespan:** For a long-duration program, the lifetime of the considered system should be high. Although no missions are yet fully planned, it is assumed that the return of humans to the Moon's surface will be permanent, as it was for the Low-Earth Orbit. With unknown duration set, it is better to promote long lifespan systems, to account for permanent presence from program starting date.
- **Potential benefits for Earth systems:** Innovation and challenges encountered by engineers, scientist and astronauts often lead to advances beyond the limits of our technologies potentially leading to spin-off Earth applications.
- **End-Of-Life:** This criterion aims to assess potential constraints due to end-of-life management of the system, decommissioning, and recyclability for other uses.

Each technology has been assessed with respect to the criteria. The detailed scoring rules, the criteria weights, their evaluation and justification are available in Appendix B. Table 3 shows the synthesis trade-off matrix.

According to the results of the trade-off analysis, the use of a TES/TEG system to power the lunar base for 66 h of darkness is not favorable with respect to other approaches. This negative result assessment is reinforced by the fact that the results were obtained in the best-case scenario, which is the unique spot of the Moon suspected to provide polar night as short as 66 h (Gläser et al., 2017). This implies that such architecture would be much less able in harsher conditions. The main drawbacks in comparison with the alternative "Solar panels and Batteries" and "Solar panels and

**Table 3**
Synthesis of the trade-off matrix for comparison of the performances of four energy production and storage systems at the rim of the Shackleton Crater (66 h of polar night): Good (++); Medium (+); Bad (-); Very Bad (X). Baseline requirement is a power demand of 10 kW.

| Criteria/Systems | Solar Panels & Batteries | Solar Panels & Fuel Cells | Fission Surface | Thermal Energy Storage |
|---|---|---|---|---|
| Mass to be delivered from Earth | - | + | + + | x |
| Specific Power | - | + | + + | x |
| Space Heritage | + + | + + | + | - |
| System Complexity | + + | - | x | + |
| Installation Efforts on the Moon | + + | + | + | x |
| Operations | + + | + + | - | + + |
| Scalability (up and down) | + + | + | + | - |
| Lifespan | + | + | - | + + |
| Potential benefit for Earth energy | + | + + | - | + |
| End-of-life (recyclability, constraints?) | - | - | x | + |
| **Total Figure of Merit** | **85** | **80** | **46** | **28** |

Regenerative Fuel Cells" are:

- Need of significant mass to be transported from Earth although ISRU activities take place (reflectors, Fresnel lens, TEG, aluminum plates, radiators). We estimated the delivered mass for one TES/TEG unit at 198 kg (see mass budget in appendix Table B3). Since it is computed that 420 units are required, the mass to be delivered to the Moon surface is about 82 tons for 10 kW of power demand. This is greater than for all other alternatives by almost a factor 5.
- Huge efforts necessary for installation. The total mass of regolith to be sintered on the Moon has been estimated to be about 245 metric tons. In addition, all the enabling systems to deploy the TES/TEG power architecture on the Moon were not considered (comprising excavation, sintering, and connections of more than 420 TES/TEG units) which would add in reality considerable labor, costs, complexity and energy consumption for sintering.
- Lack of space heritage.

Despite the poor performance of the TES/TEG concept for the considered power requirement (10 kW), the outcome of this study is valuable because it shows that ISRU-based processes are not systematically advantageous against scenarios of Earth supplies.

## 6. Conclusions and future work

An integrated model of the TES/TEG concept has been presented in this paper. One major feature is the ability of the model to account for temperature dependent properties of the TM and TEG which was not the case in previous studies. The proposed system employs a TM of 1 m$\times$ 0.3 m $\times$ 0.65 m and $Bi_2Te_3$ thermoelectric generators. The system has been optimized to reach 36 W at the end of the 66 h of the considered polar night 2 m above the surface at the rim of the Shackleton crater.

A trade-off analysis has been conducted in order to compare the TES/TEG concept with other architectures (solar arrays and batteries, solar arrays and regenerative fuel cells, fission surface power). The trade-off ranked the proposed TES/TEG system with thermoelectricity generation as the least appropriate alternative.

This result obtained under the best-condition scenario is valuable in a period of enthusiasm towards ISRU. It shows that processes exploiting extraterrestrial materials instead of Earth supplies are not systematically attractive. In actual fact, detailed analyses are required to verify if it has merit. Likewise, the ineffectiveness of thermoelectricity suggested in this specific case, should not preclude the use of thermal energy storage in a different architecture, or for other usages and scenarios.

Therefore, a number of follow-on considerations could also be studied which would open up the idea of ISRU TES systems in a more practical application:

- Integration of more efficient heat engines (TEGs with higher efficiencies, or a Stirling engine, which has a conversion efficiency of 25–30%) (Climent et al., 2014).
- Changing the location of the TEG on the TM appears very promising. We suggest replacing the TM cover cap by a TEG array which can be moved to be in contact with the top surface of the TM. During the polar day, the TEG array is not in contact with the surface that accumulates solar energy. During the darkness period, the TEG array is retracted and placed in contact with this hot surface. The advantage is that this surface is the hottest spot at the bnning of the nighttime, it prevents radiative losses and the need of a cover cap. This approach also reduces the need of a cooling system (including potential loop heat pipes) since the cold side area radiates directly the wasted energy towards deep space. The main drawback is the need for another power system during the polar day but this can be easily overcome with high-efficiency photovoltaic panels.
- Use of a TES/TEG only as a reliable power backup system instead of a primary power supply system, or only for thermal management purposes (thermal energy reservoir as part of a thermal Wadi concept) (Jones et al., 2011; Balasubramaniam et al., 2010b).
- Modelling of a single large power Thermal Energy Storage system: a 10-kW engine, and a large-scale TM with internal fluid loop heat pipes to enhance heat transfer for storage and release (Climent et al., 2014).

## Declaration of competing interest

The authors declare that they have no known competing financial interests or personal relationships that could have appeared to influence the work reported in this paper.

## Acknowledgments

This work was carried out within the Spaceship EAC initiative, which is part of the Exploration Preparation, Research and Technology activity of ESA.

## Appendix A. Thermoelectric Materials Properties

**Table A.1**
Thermoelectric generator properties for the three selected materials Bi2Te3: (Termo-Gen, 2006), PbTe/TAGS (TEC Solidstate Power Generators, 2016), and SiGe (Romanjek et al., 2015). The data obtained from the datasheet for $Bi_2Te_3$ and PbTe/TAGS are constant but from commercially available TEGs. Data on SiGe taken from (Romanjek et al., 2015). The resulting equations given for SiGe were obtained through polynomial fitting trend lines for these sources.

| Properties of TC | Value/function of temperature |
|---|---|
| $Bi_2Te_3$ (Termo-Gen, 2006) | |
| Temperature range (K) | 200 to 500 |
| Internal resistance of a TC (mΩ) | 9.75 |
| Seebeck coefficient ($\mu V.K^{-1}$) | 372.2 |
| Figure of Merit ( – ) | 0.86 |
| **PbTe/TAGS** (TEC Solidstate Power Generators, 2016) | |
| Temperature range (K) | 300 to 700 |
| Internal resistance of a TC (mΩ) | 11.4 |
| Seebeck coefficient ($\mu V.K^{-1}$) | 280 |
| Figure of Merit ( – ) | 0.85 |
| **SiGe** (Romanjek et al., 2015) | |

(*continued on next column*)

**Table A.1** (*continued*)

| Properties of TC | Value/function of temperature |
|---|---|
| Temperature range (K) | 500 to 1000 |
| n-type resistivity (Ω.m) | $-4.73\times10^{-14}\cdot T^3+7.86\times10^{-11}\cdot T^2-1.96\times10^{-8}\cdot T+2.54\times10$ |
| p-type resistivity (Ω.m) | $6.51\times10^{-12}\cdot T^2+9.75\times10^{-9}\cdot T+7.4\times10^{-6}$ |
| Seebeck coefficient ($V.K^{-1}$) | $-2\times10^{-10}\cdot T^2+6.39\times10^{-7}\cdot T+1.06\times10^{-4}$ |
| Figure of Merit ( − ) | $Z_{T\,n-type}(T_{hot})=4.286\times10^{-7}\cdot {T_{hot}}^2+7.589\times10^{-4}\cdot T_{hot}-0.1720$ |

## Appendix B. Trade-off analysis

The details of the trade-off analysis performed to compare four systems to satisfy the power demand during the polar night at the specified location are presented here. Table B1 shows the cooperative method that has been used to assign the weights to each criterion. Table B2 shows the scoring rules for each criterion. Table B3 shows the systematic approach to determine the figure of merit of each approach with respect to the proposed criteria.

**Table B1**
Trade-off weights were averaged after independent consultation of 4 researchers within the team (anonymously identified by A, B, C and D). The highest is the weight, the most it will affect the total scores.

| Criterion/Researcher preferred weights | A | B | C | D | Average Weight |
|---|---|---|---|---|---|
| Mass of the Power System | 5 | 5 | 3 | 4.5 | 4.4 |
| Global Specific Power | 1.5 | 1 | 4 | 1.5 | 2.0 |
| Space Heritage | 2 | 2 | 4 | 3.5 | 2.9 |
| System Complexity | 2.5 | 4 | 4 | 1 | 2.9 |
| Installation Efforts | 2.5 | 3 | 5 | 2.5 | 3.3 |
| Operations | 3 | 3 | 3 | 1.5 | 2.6 |
| Scalability | 2 | 1 | 3 | 4 | 2.5 |
| Lifespan | 3 | 4 | 5 | 4.75 | 4.2 |
| Potential benefit for Earth | 0.5 | 1 | 1 | 0.25 | 0.7 |
| End-of-life | 1 | 2 | 1 | 0.25 | 1.1 |

**Table B2**
Trade-off scoring rules. Each system scores +5; +3; +0 or −3 points per criterion depending on the scoring rules. The total score is calculated with a weighted average.

| Criteria/Scoring (points) | | Good (+5) | Medium (+3) | Bad (0) | Very Bad (−3) |
|---|---|---|---|---|---|
| Power System Mass | [kg] | <10000 | 10000–20000 | 20000–30000 | >30000 |
| Global Specific Power | [$W.kg^{-1}$] | >2 | 2–1 | 1–0.25 | <0.25 |
| Space Heritage | TRL | 6 or + | 4–5 | 2–3 | 1 |
| System Complexity | [see index] | 1 or less | 2–3 | 4–5 | >5 |
| Installation Efforts | [see index] | 0 | 1–2 | 3–4 | 5 |
| Operations | [see index] | 1 or less | 2–3 | 4 | >4 |
| Scalability | [ - ] | 5W - 100 kW | High-power only | low-power only | no |
| Lifespan | [years] | >15 | 10–15 | 4–10 | <4y |
| Potential benefit for Earth | [ - ] | Strong | Possible | Unlikely | No |
| End-of-life | [see index] | 3 | 2 | 1 | 0 |

**Table B3**
Criteria assessment and justifications

| |
|---|
| Power System Mass<br>All masses were estimated using the internal ESA mass budget tool. The given figures include a safety factor of 1.5 to applied on the energy storage requirement. |
| 1 Solar Arrays & Batteries: **17867 kg (bad)** i. 222 kg of solar arrays<br>ii. 14667 kg of batteries (Li-ion)<br>iii. 2978 kg for harness, structure, and power control and distribution unit<br>2 Solar Arrays & Regenerative Fuel Cells: **6507 kg (Medium)** i. 1256 kg of solar arrays<br>ii. 211 kg of electrolyzers<br>iii. 40 kg of fuel cells<br>iv. 4750 kg of hydrogen and oxygen tank dry mass<br>v. 250 kg of power control and distribution unit.<br>vi. (optional 1600 kg of water that could be brought from Earth or mined on the moon)<br>3. Fission Surface Power: **3700 kg (Good)**<br>No storage required<br>4. Thermal Energy Storage: **83205 kg (Very Bad)** i. 420 TES/TEG units required<br>ii. 2 Hot sink plate per unit: 3.24 kg<br>iii. Thermal beam per unit: 8.1 kg<br>iv. $5m^2$ radiator per unit: 33.75 kg<br>v. $21m^2$ Fresnel lens per unit: 84 kg<br>vi. 30 $m^2$ reflectors per unit: 30 kg<br>vii. Heat Pipes per unit: 6 kg<br>viii. Holding Structure, sun-trackers, Power control distribution unit (optimistic 20%): 33 kg<br>ix. Total is 198 kg per unit |

(*continued on next column*)

**Table B3** (*continued*)

Power System Mass
All masses were estimated using the internal ESA mass budget tool. The given figures include a safety factor of 1.5 to applied on the energy storage requirement.

**Global Specific Power**
1. Solar Arrays & Batteries: **0.56 W/kg (Bad)**
2. Solar Arrays & Regenerative Fuel Cells: **1.54 W/kg (Medium)**
3. Fission Surface Power: **2.7 W/kg (Good)**
4. Thermal Energy Storage: **0.12 W/kg (Very Bad)**

**Space Heritage**
1. Solar Arrays & Batteries: **TRL 9 (Good)**
2. Solar Arrays & Regenerative Fuel Cells: **TRL 6+ (Good)**
3. Fission Surface Power: **TRL 4 (Medium)**
4. Thermal Energy Storage: **TRL 2–3 (Bad)**

**System Complexity (high index is bad)**
The scoring rules refers to a system complexity index computed by addition of the points recommended if applicability of the following statement:

- Slow-motion or occasionally moving parts? (+1)
- High-velocity moving parts? (+3)
- Non-hazardous, easy to store working fluid? (+1)
- One hazardous, difficult to store working fluid? (+2)
- Multiple working fluids? (+3)
- Considerable vibrations? (+1)
- Tendency to be unstable, uncontrollable (+1)

1. Solar Arrays & Batteries: **complexity index = 1 (Good)**
2. Solar Arrays & Regenerative Fuel Cells: **complexity index = 4 (Bad)**
3. Fission Surface Power: **complexity index = 8 (Very Bad)**
4. Thermal Energy Storage: **complexity index = 2 (Medium)**

**Installation Efforts on the Moon (high index is bad)**
The scoring rules refers to a installation index computed by addition of the points recommended if applicability of the following statement:

- A couple of hours of work, almost plug and play and can be done robotically (+0)
- Humans required on-site for installation, only a few hours of work (+1)
- Little ISRU, be can be avoided with extra-mass brought from Earth (+2)
- Significant ISRU required (+3)
- More than 300 manned hours of installation (+3)

1. Solar Arrays & Batteries: **installation index = 0 (Good)**
2. Solar Arrays & Regenerative Fuel Cells: **installation index = 2 (medium)**
3. Fission Surface Power: **installation index = 2 (medium)**
(A Fission Surface Power plant shall be installed autonomously before the arrival of the crew to minimize risks. It could be assisted by robots, or self-deployable. The fission reaction can be started only when the reactor is on-site. There are not significant installation efforts to be made, because it shall be made autonomously or robotically.)
4. Thermal Energy Storage: **complexity index = 5 (Very Bad)**
(In order to install such system with 420 units to satisfy the 10 kW power, we estimate the mass to be sintered to be 246 metric tons. This is considerable and would require specialized rover, and already utilize tremendous amount of energy in the building phase.)

**Operations (high index is bad)**
The scoring rules refers to an operations index computed by addition of the points recommended if applicability of the following statement:

- Any serious safety issue, for transportation, launch or work around the base? (+2)
- Weekly maintenance estimated > 2hrs? (+1)
- Needs of Astronauts daily intervention > 30min (+2)
- Critical, non-repairable element? (+2)
- Remote monitoring necessary from Earth? (+1)

1. Solar Arrays & Batteries: **operations index = 0 (Good)**
2. Solar Arrays & Regenerative Fuel Cells: **operations index = 1 (Good)**
(high-pressure systems to be monitored)
3. Fission Surface Power: **operations index = 4 (Bad)**
There is of course safety issue with nuclear power sources, and most of the parts in the core of the system will be neither replaceable nor repairable by astronauts, but this task will be done robotically. Due to its nature, operations performed by astronauts will be minimized if no banned. Mostly, the reactor will be monitored remotely.
4. Thermal Energy Storage: **complexity index = 1 (Good)**

**Scalability**
1. Solar Arrays & Batteries: **5W – 100 kW (Good)**
2. Solar Arrays & Regenerative Fuel Cells: **high-power mostly (Medium)**
3. Fission Surface Power: **high power only (Medium)**
4. Thermal Energy Storage: **low power only (Bad)**

**Lifespan**
1. Solar Arrays & Batteries: **10–15 years (Medium)**
Lifespan limited by the battery lifetime which represent most of the subsystem mass.
2. Solar Arrays & Regenerative Fuel Cells: **10 years (Medium)**

(*continued on next column*)

**Table B3** (*continued*)

| |
|---|
| Power System Mass<br>All masses were estimated using the internal ESA mass budget tool. The given figures include a safety factor of 1.5 to applied on the energy storage requirement. |
| 3. Fission Surface Power: 5 to 10 **(Bad)**<br>4. Thermal Energy Storage: **> 15 years (Good)** |
| **Potential benefits for Earth systems**<br>1. Solar Arrays & Batteries: **possible (Medium)**<br>2. Solar Arrays & Regenerative Fuel Cells: **strong (Good)**<br>(hydrogen very much regarded as future energy vector)<br>3. Fission Surface Power: **unlikely (Bad)**<br>4. Thermal Energy Storage: **possible (Medium)** |
| **End-of-life (high index => good)**<br>The scoring rules refers to an End-of-Life index computed by addition of the points recommended if applicability of the following statement:<br>• Significant recyclability? (+3)<br>• Little recyclability? (+2)<br>• Not recyclable but no EOL constraints? (+1)<br>• Significant EOL constraints (0)<br>1. Solar Arrays & Batteries: **1 (Bad)**<br>2. Solar Arrays & Regenerative Fuel Cells: **1(Bad)**<br>3. Fission Surface Power: **0 (Very Bad)**<br>4. Thermal Energy Storage: **2 (Medium)** |

## References


Alam, H., Ramakrishna, S., 2012. A review on the enhancement of figure of merit from bulk to nano-thermoelectric materials. Nano Energy 2, 190–212. https://doi.org/10.1016/j.nanoen.2012.10.005.

Balasubramaniam, R., Wegeng, R., Gokoglu, S., Suzuki, N., Sacksteder, K., 2010. Analysis of solar-heated thermal wadis to support extended-duration lunar exploration. In: AIAA-2009-1339.

Balasubramaniam, R., Wegeng, R., Gokoglu, S., Suzuki, N., Sacksteder, K., 2010. Extended-Duration Lunar Exploration. https://ntrs.nasa.gov/archive/nasa/casi.ntrs.nasa.gov/20100015637.pdf.

Callister, W., Rethwisch, D., 2007. Materials science and engineering: an introduction. Mater. Sci. Eng. 266–267. https://doi.org/10.1016/0025-5416(87)90343-0.

Climent, B., Torroba, O., González-cinca, R., Ramachandran, N., Griffin, M.D., 2014. Heat storage and electricity generation in the Moon during the lunar night. Acta Astronaut. 93, 352–358. https://doi.org/10.1016/j.actaastro.2013.07.024.

Colaprete, A., Schultz, P., Heldmann, J., Wooden, D., Shirley, M., Ennico, K., Hermalyn, B., Marshall, W., Ricco, A., Elphic, R.C., Goldstein, D., Summy, D., Bart, G.D., Asphaug, E., Korycansky, D., Landis, D., Sollitt, L., 2010. Detection of water in the LCROSS ejecta plume. Science 330 (80-), 463–468. https://doi.org/10.1126/science.1186986, 6003.

Colozza, A., 1991. Analysis of Lunar Regolith Thermal Energy Storage.

Córdoba, P.L., 2017. Thermal Energy Storage Demonstrator. Master's Thesis. European Astronaut Centre (ESA)/UPC.

Cremers, C.J., 1973. Thermophysical properties of Apollo 12 fines. Icarus 18, 294–303.

ESA, 2010. Buidling a Lunar Base with 3D Printing. http://www.esa.int/Our_Activities/Space_Engineering_Technology/Building_a_lunar_base_with_3D_printing. (Accessed 15 April 2019).

ESA, 2016. Moon village. http://www.esa.int/About_Us/Ministerial_Council_2016/Moon_Village. (Accessed 15 April 2019).

Fleith, P., 2017. In-Situ Approaches for Thermal Energy Storage and Thermoelectricity Generation on the Moon: Modelling and Simulation. Master's Thesis. European Astronaut Centre (ESA)/ISAE-SUPAERO.

Gläser, P., Oberst, J., Neumann, G.A., Mazarico, E., Speyerer, E.J., Robinson, M.S., 2017. Illumination conditions at the lunar poles: implications for future exploration. Planet. Space Sci. 1–9. https://doi.org/10.1016/j.pss.2017.07.006.

Heiken, G., Vaniman, D., French, B.M., 1991. Lunar Sourcenook: A User's Guide to the Moon.

B.S. Hemingway, R.A. Robie, W.H. Wilson, Specific heats of lunar soils, basalt, and breccias from the Apollo 14, 15, and 16 landing sites, between 90 and 350°K, in: Lunar Sci. Conf. 4th, SAO/NASA Astrophysics Data System (ADS), n.d.: pp. 2481–2487.

Jones, H.L., Thornton, J.P., Balasubramaniam, R., Gokoglu, S.A., Sacksteder, K.R., Whittaker, W.L., 2011. Enabling Long-Duration Lunar Equatorial Operations with Thermal Wadi Infrastructure. https://ntrs.nasa.gov/archive/nasa/casi.ntrs.nasa.gov/20110007929.pdf.

Kanimba, E., Tian, Z., 2016. Modeling of a thermoelectric generator device. InTechOpen, pp. 461–479.

Langseth, M.G., Keihm, S.J., Peters, K., 1976. Revised lunar heat-flow values. In: Lunar Sci. Conf. 7th. SAO/NASA Astrophysics Data System (ADS), Houston, Texas, pp. 3143–3171. http://articles.adsabs.harvard.edu//full/1976LPSC....7.3143L/0003169.000.html.

Lozano, A.V., 2016. Development of a Lunar Regolith Thermal Energy Storage Model for a Lunar Outpost. Master's Thesis. European Astronaut Centre (ESA)/Université Paul Sabatier Toulouse III.

Mellon, M.T., Jakosky, B.M., Kieffer, H.H., Christensen, P.R., 2000. High-resolution thermal inertia mapping from the Mars global surveyor thermal emission spectrometer. Icarus 148, 437–455. https://doi.org/10.1006/icar.2000.6503.

Mitchell, D.L., De Pater, I., 1994. Microwave imaging of mercury's thermal emission at wavelengths from 0.3 to 20.5 cm. Icarus 2–32.

R. Morrel, Thermal conductivities, tables phys. Chem. Constants. (n.d.). http://www.kayelaby.npl.co.uk/general_physics/2_3/2_3_7.html (accessed February 3, 2018).

NASA/GSFC, 2010. Multi-temporal Illumination Map of the Lunar South Pole. https://www.nasa.gov/mission_pages/LRO/multimedia/gallery/121510pole.html. (Accessed 15 April 2019).

Nicollier, C., 2019. Particle Flux in the Earth Environment.

Paige, D.A., Foote, M.C., Greenhagen, B.T., Schofield, J.T., Calcutt, S., Vasavada, A.R., Preston, D.J., Taylor, F.W., Allen, C.C., Snook, K.J., Jakosky, B.M., Murrary, B.C., Soderblom, L.A., Jau, B., Loring, S., Bulharowski, J., Bowles, N.E., Thomas, I.R., Sullivan, M.T., Avis, C., De Jong, E.M., Hartford, W., McClesse, D.J., 2010. The lunar reconnaissance orbiter diviner lunar radiometer experiment. Sp. Sci Rev. 125–160. https://doi.org/10.1007/s11214-009-9529-2.

Rapp, D., 2013. Use of Extraterrestrial Resources for Human Space Missions to Moon or Mars. Springer. https://doi.org/10.1007/978-3-642-32762-9.

Romanjek, K., Vesin, S., Aixala, L., Baffie, T., Dufourcq, J., 2015. High-performance silicon – germanium-based thermoelectric modules for gas exhaust energy scavenging. J. Electron. Mater. 44, 2192–2202. https://doi.org/10.1007/s11664-015-3761-1.

Shrunk, D., Sharpe, B., Cooper, B., Thangavelu, M., 2008. THE MOON: Resources, Future Development, and Settlement, Second. Praxis Publishing Ltd.

Tatarinov, D., Koppers, M., Bastian, G., Schramm, D., 2013. Modeling of a thermoelectric generator for thermal energy regeneration in automobiles. J. Electron. Mater. 42, 2274–2281. https://doi.org/10.1007/s11664-013-2642-8.

TEC Solidstate Power Generators, Datasheet for high efficiency Pb/TAGS TEG modules (PBTAGS-200:009A10), (n.d.). http://tecteg.com/wp-content/uploads/2016/05/PBTAGS-200.009A10.pdf (accessed April 15, 2019).

Termo-Gen, A.B., 2006. Datasheet Bismuth Telluride TEG Modules (TEP1- 12656-0.6). http://www.termo-gen.com/pdf/TEG_modules_Bi2Te3.pdf. (Accessed 15 April 2019).

Tsai, H., Lin, J., 2009. Model building and simulation of thermoelectric module using matlab/simulink. J. Electron. Mater. 39, 2105–2111. https://doi.org/10.1007/s11664-009-0994-x.

Turner, R.H., 1983. Space power system utilizing Fresnel lenses for solar power and also thermal energy storage. In: Eighteenth Intersoc. Energy Convers. Eng. Conf. American Institute of Chemical Engineers, Orlando (FL), pp. 971–976.

Vasavada, A.R., Paige, D.A., Wood, S.E., 1999. Near-surface temperatures on mercury and the Moon and the stability of polar ice deposits. Icarus 141, 179–193.

Vasavada, A.R., Bandfield, J.L., Greenhagen, B.T., Hayne, P.O., Siegler, M.A., Williams, J., Paige, D.A., 2012. Lunar equatorial surface temperatures and regolith properties from the Diviner Lunar Radiometer Experiment. J. Geophys. Res. 117, 1–12. https://doi.org/10.1029/2011JE003987.